

Design of a Flexible Wearable Smart sEMG Recorder Integrated Gradient Boosting Decision Tree Based Hand Gesture Recognition

Wei Song, *Student Member, IEEE*, Qingquan Han, Zhonghang Lin, Nan Yan, Deng Luo[✉], *Student Member, IEEE*, Yiqiao Liao, *Student Member, IEEE*, Milin Zhang[✉], *Senior Member, IEEE*, Zhihua Wang, *Fellow, IEEE*, Xiang Xie[✉], Anhe Wang, Yang Chen, and Shuo Bai

Abstract—This paper proposed a wearable smart sEMG recorder integrated gradient boosting decision tree (GBDT) based hand gesture recognition. A hydrogel-silica gel based flexible surface electrode band is used as the tissue interface. The sEMG signal is collected using a neural signal acquisition analog front end (AFE) chip. A quantitative analysis method is proposed to balance the algorithm complexity and recognition accuracy. A parallel GBDT implementation is proposed featuring a low latency. The proposed GBDT based neural signal processing unit (NSPU) is implemented on an FPGA near the AFE. A RF module is used for wireless communication. A hand gesture set including 12 gestures is designed for human-computer interaction. Experimental results show an overall hand gesture recognition accuracy of 91%.

Index Terms—Flexible, FPGA, gradient boosting decision tree(GBDT), hand gesture, Neural Signal Processing Unit (NSPU), smart sEMG recorder.

I. INTRODUCTION

HAND gesture is one of the common methods for communication between human beings. For example, sign language is widely used by people with speech impairment. Automotive hand gesture recognition can be used as a Human-Machine-Interface [1]–[3] enabling a more natural and more efficient solution for information exchange between user and

devices than by using traditional methods, such as mouse and/or keyboard. Different methodologies have been proposed in literature for hand gesture recognition. The reported methods can be divided into two categories: vision-based methods, and non-vision-based methods. Vision-based methods use one or more cameras to capture image or video stream of the user's hands with no wearable devices [4]. Both standard color image sensor and infrared image sensor have been used in reported applications, such as Kinect [5] and Leap Motion [6]. Image-based feature extraction will be applied for hand gesture recognition. A high recognition accuracy performance usually can be expected. However, the use of external cameras limits the portability and/or the moving range of the user. In addition, it is usually sensitivity to environmental factors, such as the change of the illumination. Data glove is widely used as a non-vision-based hand gesture recognition device [7], [8]. Different types of sensors are usually implemented in the glove, such as the flex sensor and/or the piezoelectric sensor for the detecting of the joint bending, and the IMUs for the detecting of finger segment movement [9]. Compare to the vision-based method hand gesture recognition, the complexity of the recognition algorithm is relatively low. However, a glove is always required, which may influence the hand movement and/or cause an uncomfortable user experience.

Electromyography (EMG) is an electrical signal origins from the skeletal muscle activities [10]. It can be acquired either invasively or non-invasively. Non-invasive EMG can be acquired from the surface of the skin, which is also called surface EMG (sEMG) [11]. The movement of hand/finger is mainly controlled by the muscles located on the lower arm. Hand gesture recognition based on the sEMG signals acquired from the lower arm has been widely investigated. Typical sEMG based signal acquisition and/or feature recognition devices are fully wearable with no limitation to the user's moving range. The sEMG sensors are usually placed on the user's lower arm, with almost no burden on the movement of the hand while compare to data glove as mentioned above. In addition, this methodology enables a potential to be applied for an assistant device for hand disabled patients.

Fig. 1 illustrates a block diagram of a typical smart sEMG recorder. It consists of 1) a tissue interface which feeds sEMG signals into the electronic system, 2) a sensor interface which

Manuscript received July 15, 2019; revised September 21, 2019; accepted October 18, 2019. Date of publication November 18, 2019; date of current version December 31, 2019. This work was supported in part by the Beijing Innovation Center for Future Chip, in part by the Beijing National Research Center for Information Science and Technology, and in part by the National Natural Science Foundation of China under Grant 61674095. This paper was recommended by Associate Editor Prof. M. Ghovanloo. (*Wei Song and Qingquan Han contributed equally to this work.*) (*Corresponding author: Milin Zhang.*)

W. Song, Z. Lin, and M. Zhang are with the Department of Electronic Engineering, Tsinghua University, Beijing 100084, China (e-mail: swl7@mails.tsinghua.edu.cn; linzh16@mails.tsinghua.edu.cn; zhangmilin@tsinghua.edu.cn).

Q. Han, A. Wang, Y. Chen, and S. Bai are with the State Key Laboratory of Biochemical Engineering, Institute of Process Engineering, Chinese Academy of Sciences, Beijing 100084, China (e-mail: hanqingquan@ipe.ac.cn; ahwang@ipe.ac.cn; chenyang@ipe.ac.cn; baishuo@ipe.ac.cn).

N. Yan is with the Department of Automation, Tsinghua University, Beijing 100084, China (e-mail: yann17@mails.tsinghua.edu.cn).

D. Luo, Y. Liao, Z. Wang, and X. Xie are with the Institute of Microelectronics, Tsinghua University, Beijing 100084, China (e-mail: luod14@mails.tsinghua.edu.cn; liaoyq14@mails.tsinghua.edu.cn; zhihua@tsinghua.edu.cn; xiexiang@tsinghua.edu.cn).

Color versions of one or more of the figures in this article are available online at <http://ieeexplore.ieee.org>.

Digital Object Identifier 10.1109/TBCAS.2019.2953998

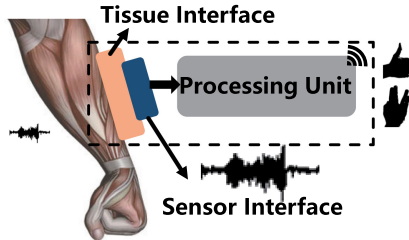


Fig. 1. The block diagram of a general smart sEMG recorder. It consists of 1) a tissue interface which feeds sEMG signals into the electronic system, 2) a sensor interface which amplifies and quantizes the acquired sEMG signal, 3) a processing unit.

amplifies and quantizes the acquired sEMG signal, and 3) a processing unit for further feature extraction and/or classification.

There are several commercial available sEMG acquisition equipments, such as Biometrics [12] and Delsys [13]. Commercial available device based hand gesture recognition has been reported in literature [14], [15]. However, there is still room to further reduce the size of the wearable devices, and/or to further simplify the using process. Customized sEMG devices have also been proposed in literature, with reported recording device size varying from tens of centimeters to a few centimeters [16]–[23]. In addition, different types of electrodes have been selected for sEMG recording, including dry electrodes of different materials, and wet electrodes such as separate disposable Ag-AgCl electrodes with gel. The use of separate electrodes cause extra process on wearing the device. Armband with fixed electrodes is available [24]–[27], but there is still room to improve the system design.

The algorithm used for hand gesture classification is important in such a smart sEMG recorder design. Various classification algorithms have been proposed in literature. Deep learning is popular in the recent years due to its high performance. Several different architectures have been proposed for hand gesture recognition [28]–[30] to improve the precision. However, the complexity of such an algorithm is relative high, which makes it very power hungry [31]. In addition, most of the deep learning based sEMG signal processing and/or recognition algorithms are verified and performed off-line, which greatly limits the application flexibility. On the other hand, traditional pattern recognition methods, such as Support Vector Machines (SVM) [32], [33], decision tree [34], naïve bayes [25], Empirical Mode Decomposition (EMD) [14], Principal Component Analysis (PCA) [35], K-Nearest Neighbors (KNN) [19], Hidden Markov Model (HMM) [22], Artificial Neural Network (ANN) [17], linear regression [15], Linear Discriminant Analysis (LDA) [36], have also been applied to hand gesture recognition. These traditional methods shows a comparable performance in several sEMG dataset, with a low requirement of training data. However, the performance is usually sensitive to the selection of the features. A robust hardware-friendly algorithm which can be implemented near amplifier without performance decrease is expected. Gradient Boosting Decision Tree (GBDT) is a boosting algorithm based on several weak decision tree classifiers [37]. It features a low dependance on the feature selection [38]. In addition, GBDT doesn't require complicated

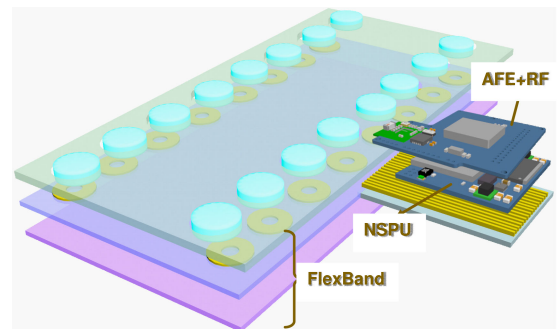


Fig. 2. The exploded diagram of the proposed smart sEMG recorder. It consists of a flexible surface electrode band, an analog front end chip, a FPGA based NSPU, and a RF module for wireless configuration and communication. The flexible surface electrode consists of three layers: 1) the conductive hydrogel-silica gel layer as the tissue interface, 2) the flexible printed circuit (FPC) layer connected to the proposed electronic system, and 3) the non-woven fabric layer.

calculation, making it hardware friendly for a wearable smart sEMG recorder.

This paper proposed a GBDT based hand gesture recognition algorithm, which is implemented in a hydrogel-silica gel, flexible wearable smart sEMG recorder. A GBDT based hand gesture recognition algorithm enabling online processing with low hardware complexity is proposed. A quantitative analysis is applied to perform a best trade-off between complexity and accuracy. A near amplifier online neural signal processing unit (NSPU) is design to perform the GBDT based algorithm achieving a good balance between cost and accuracy. The NSPU is verified on a FPGA platform near the recorder. The recognition result output from the NSPU can be wirelessly sent to external hardwares. A sEMG dataset with 12 different gestures are established using the proposed setup. An overall accuracy of 90.7% is achieved. A flexible band where the original EMG signal collect from is designed, in order to increase the usability.

The rest of the paper is organized as follows. Section II presents an overview of the proposed system. Section III describes the design of the human-computer-interface hand gesture set and the GBDT based hand gesture recognition algorithm. The details on the hardware implementation is introduced in Section IV. Experimental results was illustrated in Section V, while Section VI concludes the entire work.

II. SYSTEM OVERVIEW

Fig. 2 illustrated the architecture of the proposed smart sEMG recorder. It consists of a flexible surface electrode band, an analog front end chip, an FPGA based NSPU, and a RF module for wireless configuration and communication.

The flexible surface electrode band integrated 32 contacts is used as a tissue interface between the human skin and electronic devices. Fig. 2 demonstrated the procedure of the design of the surface electrode band. The flexible surface electrode band consists of three layers: 1) the conductive hydrogel-silica gel (CHSG) as the top layer, 2) a flexible printed circuit (FPC) layer embedded in the middle, and 3) non-woven fabric at the bottom. The conductive gel is formed by in-situ reaction. The silica gel was punched to obtain the corresponding holes to

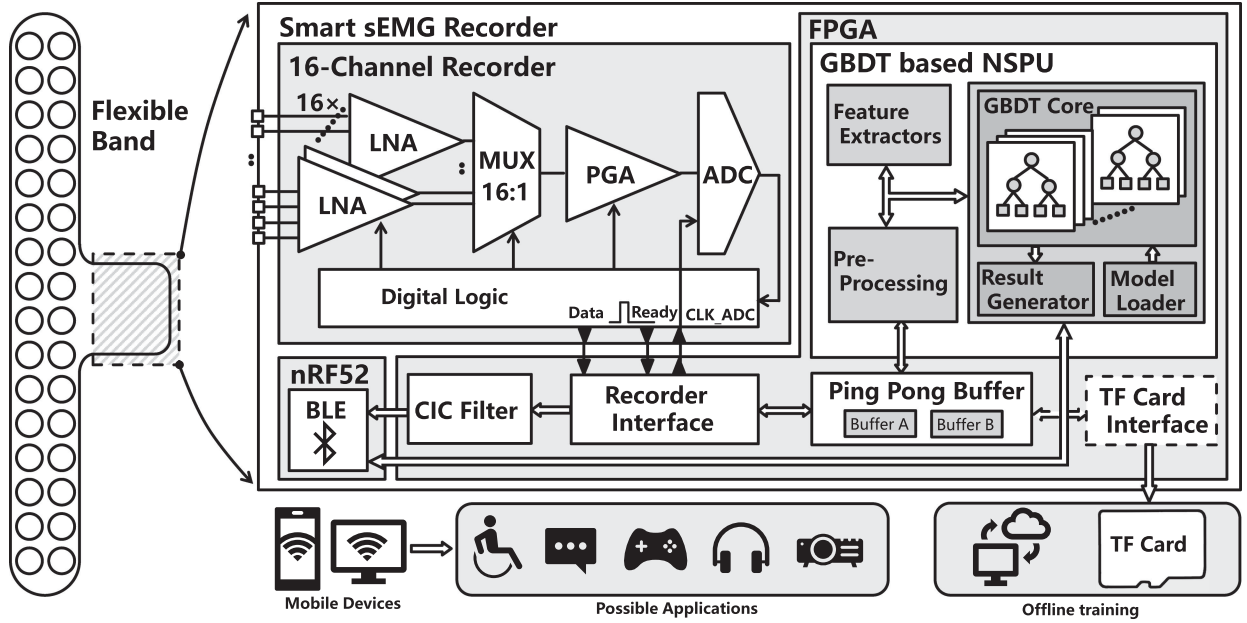


Fig. 3. Blockgram of the proposed smart sEMG recorder design.

match the electrode points on the FPC board. Subsequently, the pre-gel solution was injected into the holes on the silica gel to allow the reaction carrying on for 4.5 hours at 98 °C under acidic conditions to get CHSG. Then the CHSG, the FPC and the non-woven fabric were bonded to form the flexible surface electrode.

The output signals from the band are fed into a 16 channel neural signal acquisition analog front end (AFE) [39]. Fig. 3 illustrated the architecture of the entire system. The neural signal acquisition chip integrated a 16-channel low noise amplifier (LNA) as the input stage of the AFE. Each channel will be connected with two electrodes as the input of the differential LNA. The raw signal is amplified by 40 dB. Majority of the common mode noise will be eliminated at the first stage benefited from the high CMRR performance of the LNA. In order to improve the area efficiency of the analog front end, the second stage amplifier, the programmable gain amplifier (PGA), and the ADC are shared by all the channels. The gain of the PGA is tunable, enabling the gain of the two stages varying from 46 dB to 64 dB. The SAR ADC features a 12 bit resolution and a maximum sampling rate of 20 kHz for each channel. An extra multiplexer (MUX) is used for the channel control.

The sampling rate of the proposed AFE is tunable. Lower power consumption can be expected if a reasonable lower sampling rate is applied. In order to perform a high efficient signal acquisition, an analysis on sampling rate is performed. Four clips of raw sEMG signal were captured at a sampling rate of 2 KS/s for 5 seconds. Fig. 4 illustrated the waveform and its spectrogram of one of the four clips. According to the spectrogram, the majority of the energy distributed in the low frequency band. Fig. 5 calculated the accumulated spectral energy from the four sEMG signal clips. About 80% of the energy gathered in the band below 250 Hz. As a result, 500 S/s is chosen as the sampling rate in the proposed system.

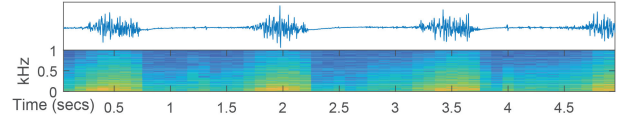


Fig. 4. The waveform and spectrogram of a 5 second raw sEMG signal acquired at a sampling rate of 2 KS/s.

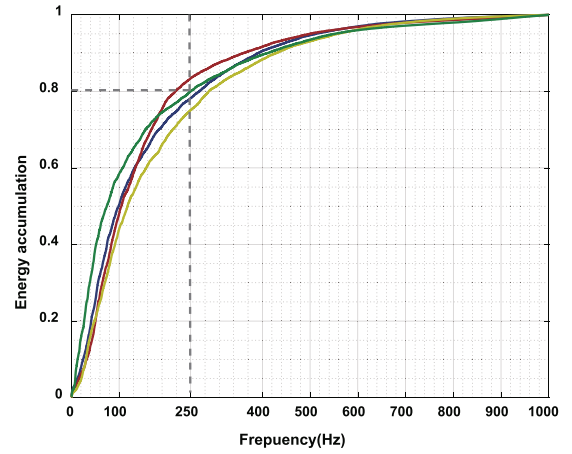


Fig. 5. The accumulated spectral energy from the four sEMG signal clips.

The digital control logic as well as the GBDT based NSPU are implemented in an FPGA. The parallel port was used for data communication between the AFE and the NSPU. A 4-bit address header is added into the 12-bit ADC output to identify the channel number of the quantized result. All the 16-bit data are packaged to fit the Serial Peripheral Interface (SPI) protocol for data writing to the TF card or the wireless channel, when raw data output is required for training purpose. Under TF card writing mode, the data from the parallel port will be buffered

in a ping-pong buffer before writing into the TF card through the SPI interface. The data prepared for TF card written can be acquired at a sampling rate as high as up to 20 kHz, enabling an acquisition of more information for off-line analysis. Under bluetooth based wireless transmission mode, a commercial Bluetooth Low Energy (BLE) module is used. Data acquired from a single selected channel with a sampling rate of 500 S/s can be transferred to the mobile device for real-time monitoring. A timestamp is also sent through the wireless channel enabling synchronization between the acquisition of the sEMG signals and other external devices.

A GBDT based hand gesture recognition algorithm is implemented. Several selected features are extracted. A pattern recognition algorithm is applied for gesture classification. The result will be sent out wirelessly through the BLE module. The details of the GBDT based NSPU design are proposed in the following sections.

III. THE GBDT BASED HAND GESTURE RECOGNITION ALGORITHM

A. The Design of the Human-Computer Interaction Gesture Dataset

The precision of the hand gesture recognition algorithm is highly related to the number of gestures to be classified [40]. As a result, The gesture set usually includes several individual gestures, and each gesture represents for one word or one instruction in their target applications. There are several open-source sEMG datasets available for hand gesture recognition. NinaPro [41], [42] is a large set including 61 gestures originally, and subsets for different targets could be selected in different scenarios. For example, CapgMyo [43] is a high density sEMG dataset which include 22 gestures equivalent to those corresponding in NinaPro. CSL-hdemg [25] is another open-source dataset for this task. 26 gestures are included in this dataset, and the ability to classify individual finger movement was shown in this work. Fig. 6 illustrated the designed gesture set, \mathcal{G} , used in this proposed work for human-computer interaction. It consists of 12 different gestures, including combinations of finger movements, and wrist involved gestures. This dataset enables user intention expression, fundamental communication between users, and/or page control during presentation.

The raw sEMG data were collected at a sampling rate of 500 S/s using the proposed system as presented in Section II, with the flexible electrode band adhered to the middle lower arm. The subjects were asked to perform repeatedly all the 12 gestures from the designed gesture set, \mathcal{G} . Each subject conducted all the 12 gestures for 10 times, and each gesture is lasted for 5 seconds. The length of each raw sEMG data clip is 5 seconds with a label identifying the corresponding gesture. The raw sEMG dataset is defined as

$$\mathcal{S} = \{(S_{i,k}, g_{i,k})\} \quad (1)$$

where $S_{i,k}$ is a matrix with 16 rows representing signals acquired from 16 channels for the i th clip of the k th subject, and $g_{i,k} \in \mathcal{G}$ is the gesture label for this clip.



Fig. 6. The selected gesture set. This dataset consists of 12 different gestures, enabling user intention expression, fundamental communication between users, and/or page control during presentation.

B. Feature Extraction of the Raw Acquired sEMG data

Each raw data clip, $S_{i,k}$, was divided into several segments using a sliding window with a length of 100 ms. There is an overlap of 50 ms between two neighboring segments. The segmented raw sEMG dataset is defined as

$$\mathcal{S}' = \{(s_{j,k}, g_{j,k})\} \quad (2)$$

where $s_{j,k}$ is the data of the j th segment, and $g_{j,k} = g_{i,k}$ if the j th segment is obtained from the i th clip.

Different features have been proposed in literature for sEMG [29]. The extracted features, instead of the raw sEMG data, were usually used as the input to different pattern recognition algorithms. According to the mathematics theory behind each feature extraction methodology, the extracted features can be classified into four categories as

- 1) **Time domain related features**, which are widely used in classical pattern recognition with low complexity. The features are directly calculated from the time-domain data.
- 2) **Autoregression coefficients**, which can be estimated from the sEMG data, revealing some characteristics of the muscle activity.
- 3) **Frequency domain features**, which are extracted after frequency domain transfer, i.e. Fourier transform.
- 4) **Wavelet transformation and others**, which are extracted after domain transfer other than traditional frequency domain transfer, i.e. a variety of different wavelet, and Hilbert-Huang transfer.

Time domain features are selected in the proposed work due to its low complexity. It enables lower requirement in hardware implementation. 9 time domain related features are selected

TABLE I
THE SELECTED FEATURES

1	Mean absolute value (MAV)	$\frac{1}{N} \sum_{t=1}^N x_t $
2	Simple square integral (SSI)	$\sum_{t=1}^N x_t ^2$
3	Minimum value (MIN)	$\min x_t$
4	Maximum value (MAX)	$\max x_t$
5	Standard deviation (STD)	$\sqrt{\frac{1}{N} \sum_{t=1}^N (x_t - \bar{x})^2}$
6	Average amplitude change (AAC)	$\frac{1}{N-1} \sum_{t=1}^{N-1} \Delta_t , \Delta_t = x_{t+1} - x_t$
7	Zero crossing (ZC)	$\sum_{t=1}^{N-1} \text{diff}(\text{sgn}(x_{t+1}), \text{sgn}(x_t))$
8	Slope sign change (SSC)	$\sum_{t=1}^{N-2} \text{diff}(\text{sgn}(\Delta_{t+1}), \text{sgn}(\Delta_t))$
9	Willison amplitude (WAMP)	$\sum_{t=1}^{N-1} u(x_{t+1} - x_t - \text{threshold})$

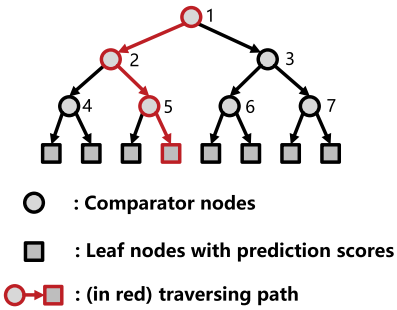


Fig. 7. An example of a single decision tree used in the GBDT model with a depth of 3. Each circle represents one comparator node, which performs comparison with a preset threshold. Each square node is a leaf node owning a predicted score for one specific gesture.

and calculated for each channel, generating $m = 9 \times 16 = 144$ features for each segment. The selected features are shown in Table I. A feature vector $z_{j,k} \in \mathbb{R}^m$ was generated for the j th segment of the k th subject. The dataset directly used by the classification algorithm was generated, which can be represented as $\mathcal{D} = \{(z_{j,k}, g_{j,k}) | z_{j,k} \in \mathbb{R}^m, g_{j,k} \in \mathcal{G}\}$.

C. The GBDT Based Classification Algorithm

Gradient Boosting Decision Tree (GBDT) is used in this work for classification due to its low complexity. GBDT is a boosting algorithm using decision trees as its base weak learner. The GBDT model, \mathcal{F} , is a set of classification and regression trees (CART). Each individual tree in the set \mathcal{F} is a binary tree as illustrated in Fig. 7. Each circle represents one comparator node, which performs comparison between the input and a preset threshold. The input is one of the m extracted features. Each

square node is a leaf node with a predicted score for one specified gesture, which represents a probability of this gesture to be the true gesture for this sample. The set \mathcal{F} is composed of several subsets \mathcal{F}_g , which includes trees for the gesture g . Given a feature vector $z_{j,k}$, an additive assembling model is used, to get a predicted score for each gesture as:

$$\hat{p}_{j,k}^{(g)} = \sum_{f \in \mathcal{F}_g} f(z_{j,k}) \quad (3)$$

which means the predict score for one gesture $\hat{p}_{j,k}^{(g)}$ is the summation of the predict scores obtained from all the trees in \mathcal{F}_g .

After all the trees for all the gestures have been traversed, and the predicted scores for every gesture have been calculated, the largest predicted score will be the final prediction, which can be generated as:

$$\hat{g}_{j,k} = \arg \max_g \hat{p}_{j,k}^{(g)} \quad (4)$$

where $\hat{g}_{j,k}$ is the predicted gesture for the j th segment of the k th subject. If $\hat{g}_{j,k} = g_{j,k}$, the prediction is correct.

The threshold assigned to each comparator node, and the predicted score on each leaf node can be optimized by training. The structure of a GBDT model, including the total number of trees and their maximum depth are decided during the training as well. [44] The training of GBDT is an iteration process. In each iteration, a new tree will be obtained in a gradient descent manner using logarithmic loss function for each gesture. As a result, the number of trees in the set \mathcal{F}_g for each gestures is equal to the iteration round K , and the total number of trees in \mathcal{F} is $12 \times K$. There are several open source library for the training of a GBDT model offline on a PC or a server, such as XGBoost [45], LightGBM [46]. XGBoost library was selected in this work for model training.

There is a trade-off between the recognition accuracy and the model complexity. A quantitative analysis is performed between the maximum tree depth and the recognition accuracy, as well as between the category tree number and the recognition accuracy, based on the NInapro dataset to provide a general analysis. As illustrated in Fig. 8(a), five different category tree numbers, K , were selected, in order to find a common turning point on the accuracy versus tree depth curve. According to the results, a common tuning point at around 5 is observed. Fig. 8(b) shows the relationship between the accuracy and the total tree number for each gesture, K . The maximum tree depth was fixed to 5. A turning point was observed around 80. A quantitative analysis has also been applied on the dataset acquired using the hardware proposed in this work. As illustrated in Fig. 8(c), the depth of 5 is also suitable for the proposed dataset. In addition, the accuracy of the depth of 4 or 3 is not significantly lower, which shows a possibility to further shallower the structure. As illustrated in Fig. 8(d), the tree number of 100 performed better than 80. However, the accuracy gap is less than 0.5%. According to the above quantitative analysis, an optimized tree depth is fixed to 5, with a tree number fixed to 80 for the model training in this work.

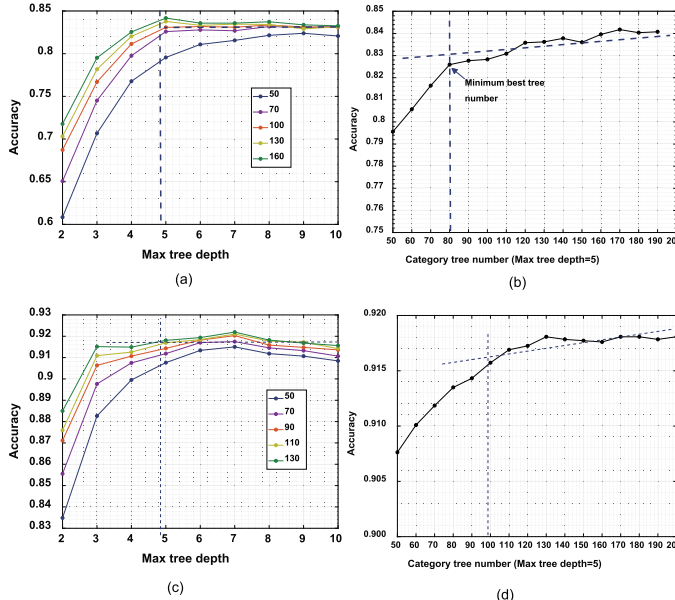


Fig. 8. (a) Quantitative analysis on the relationship between the maximum tree depth and the recognition accuracy. The category tree number, K , is equal to 50, 70, 100, 130 and 160 for each line, respectively. A common turning point at around 5 is observed. (b) Quantitative analysis on the relationship between the category tree number and the recognition accuracy. The depth of the tree was fixed to 5. A common turning point at around 80 is observed. (c, d) Quantitative analysis using the proposed dataset in this work.

IV. HARDWARE IMPLEMENTATION OF THE GBDT BASED NSPU

The training of the GBDT model was operated offline, while the inference procedure of a pre-trained GBDT model was implemented in FPGA. Fig. 11 shows the architecture of the proposed GBDT based NSPU. In order to reduce the latency of tree traversing, a parallel traversing method was proposed in this paper. A pipeline structure is used to increase hardware efficiency for traversing of different trees.

A. Implementation of the Parallel Traversing Tree

Traditional tree traversing visits the root node firstly. The child nodes are visited according to the comparison results from a higher layer. The latency is proportional to the depth of the tree [47]. In order to reduce the traversing latency, instead of exploring a path from the root node to the leaf nodes layer by layer, a parallel traversing was applied in this work. The comparison of all the leaf nodes are performed at the same time.

For a tree with a depth of n , 2^n predicted scores are output. There are $2^n - 1$ comparison modules required, as illustrated in the dotted block in Fig. 11. A threshold loaded from the memory and a selected feature are fed into the comparator. The thresholds of all the comparators are loaded simultaneously in one clock cycle. A predicted score is selected as the output according to the results of the comparators.

Fig. 9 present an example on how to perform the parallel traversing tree methodology to a tree with a depth of 3. There are seven comparator nodes integrated in this tree. A truth table was generated with different combinations of the comparison results

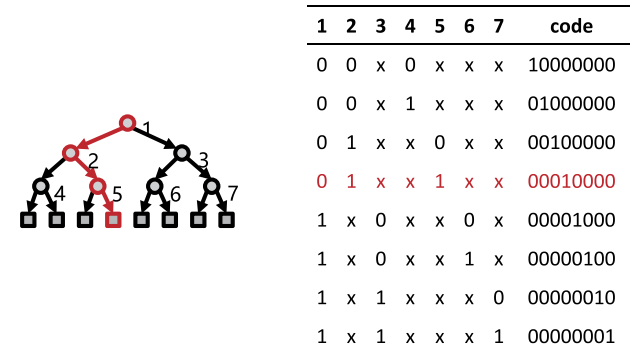


Fig. 9. An example truth table for a 3-depth tree traversing. If the output address is 00010000, the predict score attached to the right child of node 5 will be output. The traversing path is highlighted in red.

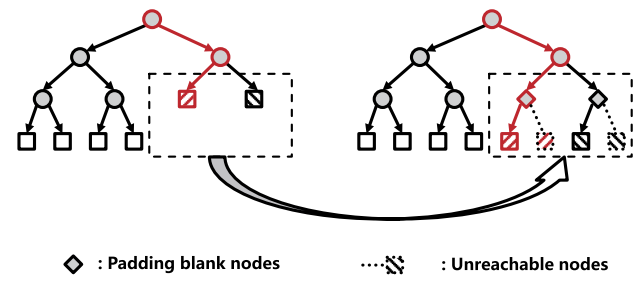


Fig. 10. Padding irregular trees.

from all the seven nodes. An 8-bit one-hot address code is used to denote the predict scores as listed on the right. The comparator results are presented in 0/1, representing a movement to the left child node, or the right child node, respectively. The pre-coded results can be used to select a predict score. For example, with an output address of 00010000, the predict score on the right child node of node 5 will be the output. The traversing path is highlighted in red.

B. Padding of the Pruned Trees

In order to avoid overfitting of a GBDT model, pruning is applied during the training procedure [48]. As a result, the tree structure is sometimes incomplete as illustrated in Fig. 10(a). The pruned tree structures may lead to abnormalities in the arrangement of node comparators, and/or score address generating module. In order to improve the robustness of the system, virtual nodes are added to the pruned locations as illustrated in Fig. 10(b). These virtual nodes will generate a fake "comparison result" always leading to the left child node with the same predicted score as the original score of the virtual node. As illustrated in the dotted block in Fig. 11, the results of the comparators are directly controlled if it is a virtual node.

In order to keep consistency during the tree generation procedure between the regular tree and the pruned tree, level traversal will be used. A reference full binary tree is used to generate a padded binary tree from its original irregular structure. As shown in Fig. 12, the reference tree is traversed simultaneously with the target tree, providing a reference full structure for generating.

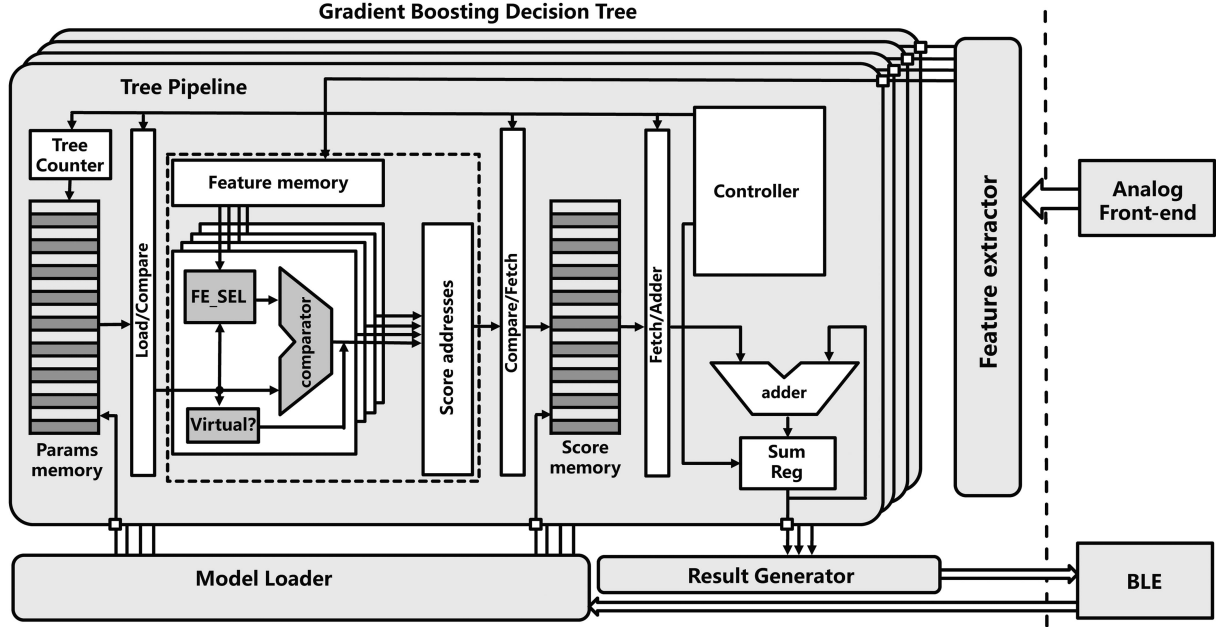


Fig. 11. Architecture of the proposed GBDT based NSPU. The recorded sEMG data are fed into the feature extraction module from the analog front end. A start signal will be sent to all the parallel tree pipelines for different gestures when the extracted features are ready. The result generator compares the output from all the GBDT models to find out the gesture with the maximum value.

Algorithm 1 Algorithm for generating the padded tree

Input:

The irregular tree T_i ;
the reference full binary tree T_r ;

Output:

The padded tree node list T_p in level traversal manner;

Initialization :

- 1: Establish two empty queue Q_i and Q_r ;
- 2: Push the root node n_i^1 and n_r^1 into Q_i and Q_r , respectively;
- 3: **while** $Q_r \neq \phi$ **do**
- 4: Pop a node n_i^t from Q_i to list T_p ;
- 5: Pop a node n_r^t from Q_r ;
- 6: **if** $n_r^t.\text{child}$ is not leaf and $n_i^t.\text{child}$ is leaf **then**
- 7: Push $n_r^t.\text{childs}$ into Q_r ;
- 8: Create two virtual nodes whose childs are $n_i^t.\text{child}$;
- 9: Push those virtual nodes $n_i^{t_{1/2}}$ into Q_i ;
- 10: **else if** $n_r^t.\text{child}$ is not leaf and $n_i^t.\text{child}$ is not leaf **then**
- 11: Push $n_i^t.\text{childs}$ and $n_r^t.\text{childs}$ into Q_i and Q_r ;
- 12: **else if** $n_r^t.\text{child}$ is leaf and $n_i^t.\text{child}$ is leaf **then**
- 13: Continue;
- 14: **end if**
- 15: **end while**
- 16: **return** T_p

Fig. 12. Algorithm for the generation of the padded tree.

C. Tree Pipeline

Two times of memory access were required while implementing the parallel traversing methodology, for thresholds loading and predict score loading, respectively. A pipeline, as illustrated in Fig. 13 is applied to reduce the latency due to loading.

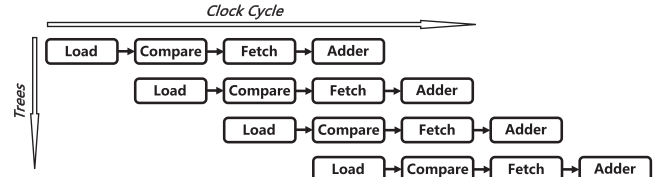


Fig. 13. The pipeline used for parallel tree traversing methodology. There are four steps in the pipeline.

The entire process of calculating the predict score of a single tree can be divided into four stages: 1) load the threshold parameters from memory, 2) compare the loaded thresholds at each node, 3) fetch a predicted score according to the comparison results, 4) add the predicted score to the sum from previous process. A finite state machine is used to control the pipeline. The pipeline won't start until the features are ready for a new frame. All the instantiated trees will be operated one by one. The final predicted score will be available after the operation to the last tree is done. Instead of calculating all the trees in one pipeline, a series of tree pipelines is established, with a total number equals to the number of gestures. By doing this, one tree pipeline is dedicated for one gesture, and only corresponding trees will be calculated in that pipeline. As a result, those tree pipelines operate in the means of parallel. As the tree number of each gestures are always the same, the results of the parallel tree pipelines will be output simultaneously.

V. EXPERIMENTAL RESULTS

Fig. 14(a) shows the photography of the proposed smart sEMG recorder. The length of the flexible band is 25.5 cm.

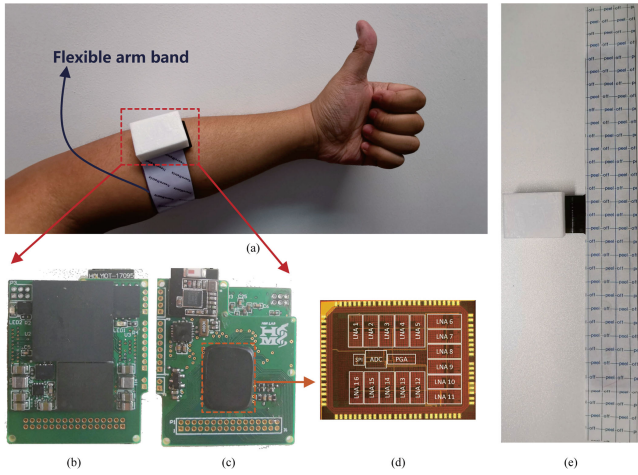


Fig. 14. (a) The photography of the proposed smart sEMG recorder. (b) the processing PCB for gesture recognition, (c) the acquisition PCB for sEMG recording, (d) The microphotography of the multiple channel analog front end chip integrated in the acquisition PCB., (e) the electrode side of the band, and (f) the outer side of the band.

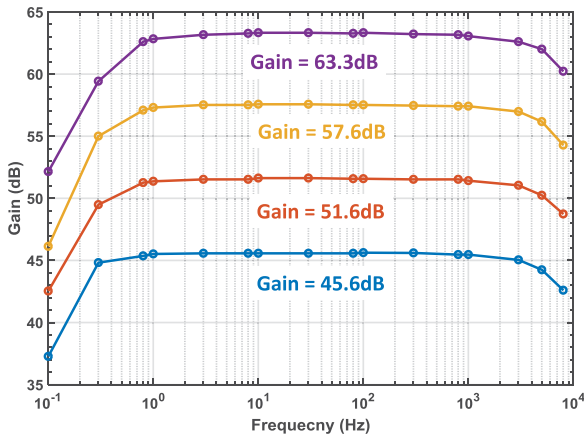


Fig. 15. The measured frequency response of the whole signal chain of the AFE chip.

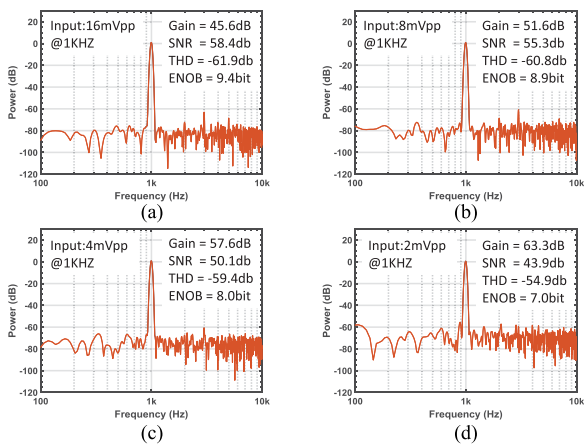


Fig. 16. The measured output spectrum of the whole signal chain of the AFE chip with different gain setting.

TABLE II
MEASURED PERFORMANCE OF THE HYDROGEL-SILICA GEL BASED ARM BAND

Conductivity	7.1 ± 0.2 E-3 S/cm
Storage moduli (stretching)	12.6 ± 1.7 kPa
(compressing)	44.2 ± 0.2 kPa
Adhesion strength	41.7 ± 3.0 kPa
Content of water	$69.6 \pm 0.2\%$
Transparency	$62.8 \pm 4.8\%$

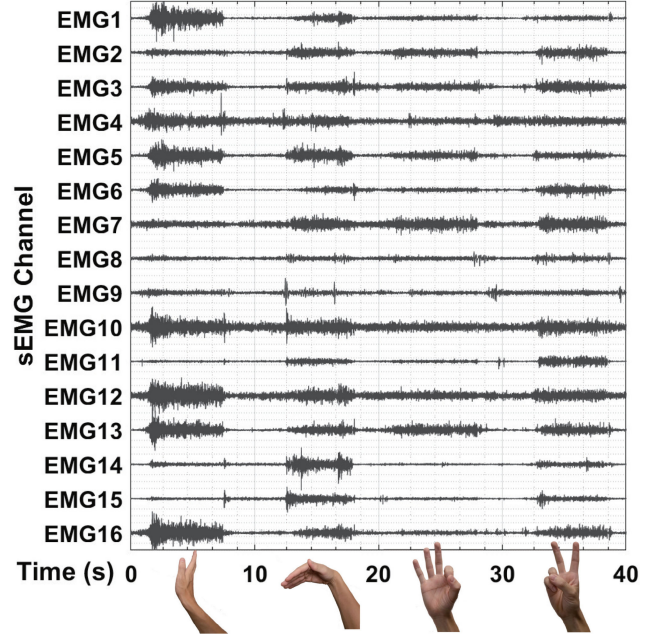


Fig. 17. An example fragment of sEMG signals and gestures.

The band is surrounding the middle place of one's lower arm to collecting sEMG signals. Two PCBs were used as shown in Fig. 14(b) and (c), respectively. Fig. 14(d) illustrated the microphotography of the multiple channel analog front end chip integrated in the acquisition PCB with a size of $2.8\text{ cm} \times 3.2\text{ cm}$. The two PCBs are sealed in a customized box with a size of $3.2\text{ cm} \times 4.3\text{ cm}$. A Xilinx Artix-7 XC7A50 T FPGA is integrated on the processing PCB. The proposed hand gesture recognition algorithm is implemented on this FPGA. Fig. 14(e) shows the connection between the flexible band and the customized box. They are attached together using a standard 1.27 mm connector, and the customized box can be folded on the outer side of the band.

The analog front end chip has been fabricated in TSMC 180 nm COMS process, occupying a silicon area of $2.6\text{ mm} \times 2\text{ mm}$. The measured frequency response of the whole signal chain with LNA, PGA and ADC is illustrated as Fig. 15 (the HP doesn't match with the amplifier). Two bits can be used to tune the gain from 45.6 dB to 63.3 dB. Fig. 16 shows the measured output spectrum of the whole signal chain. With a input of 16 mVpp at 1 KHz, when the gain is set to 45.6 db, a ENOB of 9.4 bit can be achieved. The BLE module is also placed on the top-left corner of the acquisition PCB. An nRF52832 BLE chip produced by Nordic is used for this module.

TABLE III
COMPARE WITH STATE-OF-THE-ART WEARABLE SEMG RECORDERS, SOME OF THESE ALSO DID THE TASK OF HAND GESTURE RECOGNITION

	Benatti[18]	Wu[19]	Liu[17]	Ergeneci[20]	Benatti[21]	Shaabana[22]	Cerone[23]	This work
Year	2015	2016	2017	2018	2019	2019	2019	2019
Publication	TBioCAS	JBHI	TCAS-II	TBioCAS	TBioCAS	Sens. J.	TBME	TBioCAS
Size	8.5cm×5cm	-	3.4cm×2.5cm	~10cm	~10cm	5.5cm×3.5cm	3.4cm×3cm	3.2cm×2.8cm
Electrode	Separate wet electrodes	-	Separate wet electrodes	Gold plated copper	Separate wet electrodes	Separate wet electrodes	Ag	Flexible electrode band
#Channel	8	4	4	8	8	8	32	16
AFE	Customized ASIC	Commercial ASIC	Commercial amplifier	Commercial amplifier	Commercial ASIC	Commercial ASIC	Commercial ASIC	Customized ASIC
Processor	Cortex-M4	MSP430	Cortex-M4	Cortex-M4	RISC-V	MIPS	Cortex-M4	FPGA
Tasks	HGR	Sign language	HGR	Contraction Detection	HGR	HGR	-	HGR
Algorithm	SVM	SVM	ANN	-	HDC	GM-HMM	-	GBDT
Online processing	Yes	No	Yes	-	Yes	No	No	Yes
#Gesture (If HGR)	7	-	10	-	11	5	-	12
Accuracy	89.2%	-	94%	-	85%	93%	-	91%

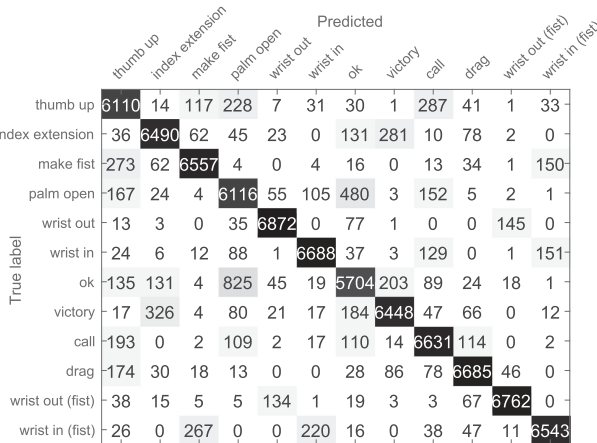


Fig. 18. The confusion matrix of the MCC results.

Table II summarizes the performance of the hydrogel-silica gel based arm band. The hydrogels with a conductivity of $7.1 \pm 0.2\text{E-}3\text{ S/cm}$ possessed an excellent storage moduli about $12.6 \pm 1.7\text{ kPa}$ (stretching) and $44.2 \pm 0.2\text{ kPa}$ (Compressing), respectively. Meanwhile the corresponding experiment certified the hydrogels had a great adhesion strength about $41.7 \pm 3.0\text{ kPa}$. In addition, the hydrogels showed a fine transparency about $62.8 \pm 4.8\%$ as the content of water was $69.6 \pm 0.2\%$.

A dataset was established using the proposed hardware. 7 right handed human subjects participated in the data collection. The armband is adhered to the subject's middle lower arm with the customized box containing the PCBs located at the thumb side of the arm. The subjects were asked to perform all the 12 gestures in turn. Each gesture was lasted for 5 seconds, with a 5 seconds for relaxation between two gestures. This procedure was repeated for 10 times by each subject. Fig. 17 shows an example fragment of the 16 channel recorded sEMG signals as well as their corresponding gestures.

To evaluate the performance of the proposed GBDT based hand gesture recognition algorithm, a Monte Carlo cross-validation (MCC) have been performed. In each run of the MCC, 70% data selected randomly to form a training set, with the remaining 30% data used as the test set. 10 runs have

TABLE IV
THE MCC RESULT METRICS

Gesture	Precision	Sensitivity	Specificity	F1-Score
Thumb up	85.1%	88.6%	98.6%	0.867
Index extension	91.5%	90.7%	99.2%	0.910
Make fist	93.1%	92.2%	99.4%	0.926
Palm open	81.2%	86.0%	98.2%	0.834
Wrist out	96.0%	96.2%	99.6%	0.961
Wrist in	94.3%	93.7%	99.5%	0.939
"OK"	83.6%	79.3%	98.6%	0.813
"Victory"	91.7%	89.3%	99.2%	0.904
"Call"	88.9%	92.2%	98.9%	0.904
"Drag"	93.5%	93.4%	99.4%	0.934
Wrist out (fist)	96.8%	95.9%	99.7%	0.963
Wrist out (fist)	95.1%	91.3%	99.6%	0.930
Overall	90.9%	90.7%	99.2%	0.907

been done, with different divisions of the dataset. An overall accuracy of 90.7% is achieved. A series of metrics, including precision, sensitivity, specificity, and F1-score, are calculated and presented in Table IV. A confusion matrix was illustrated in Fig. 18.

Table III compares the performance of the proposed work with state-of-the-art armband designs. The proposed work features a flexible armband with one of the best recognition accuracy and a compact size. The GBDT-based algorithm features lower hardware requirement.

VI. CONCLUSION

This paper proposed a compact, flexible, wearable smart sEMG recorder integrated gradient boosting decision tree based hand gesture recognition algorithm. A parallel traversing tree structure is proposed and implemented in hardware to reduce the latency. A pipeline is applied to improve the hardware efficiency. A 91% recognition accuracy is achieved on a human-computer-interface hand gesture set designed in this work.

REFERENCES

- [1] C. A. Pickering, K. J. Burnham, and M. J. Richardson, "A research study of hand gesture recognition technologies and applications for human vehicle interaction," in *Proc. 3rd Inst. Eng. Technol. Conf. Automotive Electron.*, 2007, pp. 1–15.

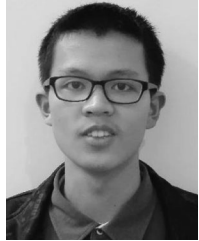
- [2] K. M. Sagayam and D. J. Hemanth, "Hand posture and gesture recognition techniques for virtual reality applications: a survey," *Virtual Reality*, vol. 21, no. 2, pp. 91–107, 2017.
- [3] C. Dong, M. C. Leu, and Z. Yin, "American sign language alphabet recognition using microsoft kinect," in *Proc. IEEE Conf. Comput. vision Pattern Recognit. Workshops*, 2015, pp. 44–52.
- [4] J. P. Wachs, M. Kölsch, H. Stern, and Y. Edan, "Vision-based hand-gesture applications," *Commun. ACM*, vol. 54, no. 2, pp. 60–71, 2011.
- [5] Kinect for windows. [Online]. Available: <https://developer.microsoft.com/en-us/windows/kinect>. Accessed on: Sep. 20, 2019.
- [6] Leap motion website. [Online]. Available: <https://www.leapmotion.com/>. Accessed on: Sep. 20, 2019.
- [7] T. F. O'Connor, M. E. Fach, R. Miller, S. E. Root, P. P. Mercier, and D. J. Lipomi, "The language of glove: Wireless gesture decoder with low-power and stretchable hybrid electronics," *PloS one*, vol. 12, no. 7, p. e0179766, 2017.
- [8] J. Gaika, M. Maśior, M. Zaborski, and K. Barczevska, "Inertial motion sensinsg glove for sign language gesture acquisition and recognition," *IEEE Sensors J.*, vol. 16, no. 16, pp. 6310–6316, Aug. 2016.
- [9] M. A. Ahmed, B. B. Zaidan, A. A. Zaidan, M. M. Salih, and M. M. b. Lakulu, "A review on systems-based sensory gloves for sign language recognition state of the art between 2007 and 2017," *Sensors*, vol. 18, no. 7, 2018, Art. no. 2208.
- [10] R. Merletti, P. A. Parker, and P. J. Parker, *Electromyography: Physiology, Engineering, and Non-Invasive Applications*. vol. 11, New York, NY, USA: Wiley, 2004.
- [11] E. Criswell, *Cram's Introduction to Surface Electromyography*. Burlington, MA, USA: Jones & Bartlett, 2010.
- [12] Biometrics ltd website. [Online]. Available: <http://www.biometricsltd.com/>. Accessed on: Sep. 20, 2019.
- [13] Delsys emg sensors. [Online]. Available: <https://www.delsys.com/trigno/sensors/>. Accessed on: Sep. 20, 2019.
- [14] C. Sapsanis, G. Georgoulas, A. Tzes, and D. Lymberopoulos, "Improving EMG based classification of basic hand movements using EMD," in *Proc. IEEE 35th Annu. Int. Conf. Eng. Medicine Biol. Soc.*, 2013, pp. 5754–5757.
- [15] L. H. Smith, T. A. Kuiken, and L. J. Hargrove, "Evaluation of linear regression simultaneous myoelectric control using intramuscular EMG," *IEEE Trans. Biomed. Eng.*, vol. 63, no. 4, pp. 737–746, Apr. 2016.
- [16] W. Jin, Y. Li, and S. Lin, "Design of a novel non-invasive wearable device for array surface electromyogram," *Int. J. Inf. Electron. Eng.*, vol. 6, no. 2, p. 139, 2016.
- [17] X. Liu, J. Sacks, M. Zhang, A. G. Richardson, T. H. Lucas, and J. Van der Spiegel, "The virtual trackpad: An electromyography-based, wireless, real-time, low-power, embedded hand-gesture-recognition system using an event-driven artificial neural network," *IEEE Trans. Circuits Syst. II, Exp. Briefs*, vol. 64, no. 11, pp. 1257–1261, Nov. 2017.
- [18] S. Benatti *et al.*, "A versatile embedded platform for EMG acquisition and gesture recognition," *IEEE Trans. Biomed. Circuits Syst.*, vol. 9, no. 5, pp. 620–630, Oct. 2015.
- [19] J. Wu, L. Sun, and R. Jafari, "A wearable system for recognizing american sign language in real-time using IMU and surface EMG sensors," *IEEE J. Biomed. Health Informat.*, vol. 20, no. 5, pp. 1281–1290, Sep. 2016.
- [20] M. Ergeneci, K. Gokcesu, E. Ertan, and P. Kosmas, "An embedded, eight channel, noise canceling, wireless, wearable sEMG data acquisition system with adaptive muscle contraction detection," *IEEE Trans. Biomed. Circuits Syst.*, vol. 12, no. 1, pp. 68–79, Feb. 2018.
- [21] S. Benatti, F. Montagna, V. Kartsch, A. Rahimi, D. Rossi, and L. Benini, "Online learning and classification of EMG-based gestures on a parallel ultra-low power platform using hyperdimensional computing," *IEEE Trans. Biomed. Circuits Syst.*, vol. 13, no. 3, pp. 516–528, Jun. 2019.
- [22] A. Shaabana, J. Legere, J. Li, R. Zheng, M. V. Mohrenschmidt, and J. M. Shedd, "Portable electromyography: A case study on ballistic finger movement recognition," *IEEE Sensors J.*, vol. 19, no. 16, pp. 7043–7055, Aug. 2019.
- [23] G. L. Cerone, A. Botter, and M. Gazzoni, "A modular, smart, and wearable system for high density sEMG detection," *IEEE Trans. Biomed. Eng.*, vol. 66, no. 12, pp. 3371–3380, Dec. 2019.
- [24] Welcome to Myo support. [Online]. Available: <https://support.getmyo.com/hc/en-us>. Accessed on: Sep. 20, 2019.
- [25] C. Amma, T. Krings, J. Böer, and T. Schultz, "Advancing muscle-computer interfaces with high-density electromyography," in *Proc. 33rd Annu. ACM Conf. Human Factors Comput. Syst.*, ACM, 2015, pp. 929–938.
- [26] M. Kim, G. Gu, K. Cha, D. Kim, and W. Chung, "Wireless semg system with a microneedle-based high-density electrode array on a flexible substrate," *Sensors*, vol. 18, no. 1, 2018, Art. no. 92.
- [27] A. Moin *et al.*, "An emg gesture recognition system with flexible high-density sensors and brain-inspired high-dimensional classifier," in *Proc. IEEE Int. Symp. Circuits Syst.*, 2018, pp. 1–5.
- [28] Y. Du, Y. Wong, W. Jin, W. Wei, Y. Hu, M. S. Kankanhalli, and W. Geng, "Semi-supervised learning for surface EMG-based gesture recognition," in *Proc. IJCAI*, 2017, pp. 1624–1630.
- [29] W. Wei, Q. Dai, Y. Wong, Y. Hu, M. Kankanhalli, and W. Geng, "Surface electromyography-based gesture recognition by multi-view deep learning," *IEEE Trans. Biomed. Eng.*, vol. 66, no. 10, pp. 2964–2973, Oct. 2019.
- [30] U. Côté-Allard *et al.*, "Deep learning for electromyographic hand gesture signal classification using transfer learning," *IEEE Trans. Neural Syst. Rehabil. Eng.*, vol. 27, no. 4, pp. 760–771, Apr. 2019.
- [31] M. Shoaran, B. A. Haghi, M. Taghavi, M. Farivar, and A. Emami-Neyestanak, "Energy-efficient classification for resource-constrained biomedical applications," *IEEE J. Emerg. Sel. Topics Circuits Syst.*, vol. 8, no. 4, pp. 693–707, Dec. 2018.
- [32] S. Benatti, B. Milosevic, F. Casamassima, P. Schönle, P. Bunjaku, S. Fateh, Q. Huang, and L. Benini, "EMG-based hand gesture recognition with flexible analog front end," in *Proc. IEEE Biomed. Circuits Syst. Conf.*, 2014, pp. 57–60.
- [33] R. Meattini, S. Benatti, U. Scarcia, D. De Gregorio, L. Benini, and C. Melchiorri, "An sEMG-based human–robot interface for robotic hands using machine learning and synergies," *IEEE Trans. Compon., Packag. Manuf. Technol.*, vol. 8, no. 7, pp. 1149–1158, Jul. 2018.
- [34] J. Wu, Z. Tian, L. Sun, L. Estevez, and R. Jafari, "Real-time american sign language recognition using wrist-worn motion and surface emg sensors," in *Proc. IEEE 12th Int. Conf. Wearable Implantable Body Sensor Netw.*, 2015, pp. 1–6.
- [35] C. Sapsanis, G. Georgoulas, and A. Tzes, "Emg based classification of basic hand movements based on time-frequency features," in *Proc. IEEE, 21st Mediterranean Conf. Control Autom.*, 2013, pp. 716–722.
- [36] C. W. Antuvan and L. Masia, "An LDA-based approach for real-time simultaneous classification of movements using surface electromyography," *IEEE Trans. Neural Syst. Rehabil. Eng.*, vol. 27, no. 3, pp. 552–561, Mar. 2019.
- [37] J. H. Friedman, "Greedy function approximation: A gradient boosting machine," *Ann. Statistics*, vol. 29, no. 5, pp. 1189–1232, 2001.
- [38] A. J. Ferreira and M. A. Figueiredo, "Boosting algorithms: A review of methods, theory, and applications," in *Ensemble Machine Learning*. Berlin, Germany: Springer, 2012, pp. 35–85.
- [39] D. Luo, M. Zhang, and Z. Wang, "A low-noise chopper amplifier designed for multi-channel neural signal acquisition," *IEEE J. Solid-State Circuits*, vol. 54, no. 8, pp. 2255–2265, Aug. 2019.
- [40] M. Atzori, M. Cognolato, and H. Müller, "Deep learning with convolutional neural networks applied to electromyography data: A resource for the classification of movements for prosthetic hands," *Front. Neurorobot.*, vol. 10, 2016, Art. no. 9.
- [41] M. Atzori, A. Gijsberts, S. Heynen, A.-G. M. Hager, O. Deriaz, P. Van Der Smagt, C. Castellini, B. Caputo, and H. Müller, "Building the ninapro database: A resource for the biorobotics community," in *Proc. 4th IEEE RAS & EMBS Int. Conf. Biomed. Robot. Biomechatron.*, 2012, pp. 1258–1265.
- [42] M. Atzori, A. Gijsberts, C. Castellini, B. Caputo, A.-G. M. Hager, S. Elsig, G. Giatsidis, F. Bassetto, and H. Müller, "Electromyography data for non-invasive naturally-controlled robotic hand prostheses," *Scientific Data*, vol. 1, 2014, Art. no. 140053.
- [43] Y. Du, W. Jin, W. Wei, Y. Hu, and W. Geng, "Surface emg-based inter-session gesture recognition enhanced by deep domain adaptation," *Sensors*, vol. 17, no. 3, 2017, Art. no. 458.
- [44] Xgboost documentation. [Online]. Available: <https://xgboost.readthedocs.io/en/latest/>. Accessed on: Jul. 14, 2019.
- [45] T. Chen and C. Guestrin, "Xgboost: A scalable tree boosting system," in *Proc. 22nd ACM Sigkdd Int. Conf. Knowl. Discovery Data Mining*, ACM, 2016, pp. 785–794.
- [46] G. Ke, Q. Meng, T. Finley, T. Wang, W. Chen, W. Ma, Q. Ye, and T.-Y. Liu, "Lightgbm: A highly efficient gradient boosting decision tree," *Advances Neural Inf. Process. Syst.*, pp. 3146–3154, 2017.
- [47] Y. R. Qu and V. K. Prasanna, "Compact hash tables for decision-trees," *Parallel Comput.*, vol. 54, pp. 121–127, 2016, 26th International Symposium on Computer Architecture and High Performance Computing.
- [48] E. Frank, "Pruning decision trees and lists," Ph.D. dissertation, Dept. Comp. Sci., Univ. Waikato, Waikato, New Zealand, 2000.



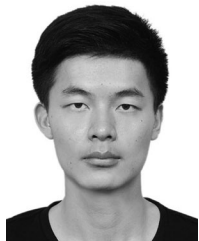
Wei Song (S'17) received the B.S. degree in electronic engineering from Tsinghua University, Beijing, China, in 2017. He is currently working toward the Ph.D. degree with Tsinghua University. His current research interests include brain-machine-interface system design, and low power biomedical signal processing algorithm design.



Qingquan Han received the B.S. degree in School of Biotechnology from the Jiangnan University, Jiangsu, China, in 2018. He is currently working toward the M.S. degree with the Institute of Process Engineering, Chinese Academy of Sciences, focusing on conductive hydrogel and wearable bioelectronics designing. His current research interests include the designing and synthesis of novel polymer-based hydrogel, and fabrication of conductive materials.



Zhonghang Lin is currently working as a senior student in the Electronic Engineering Department, Tsinghua University, Beijing, China.



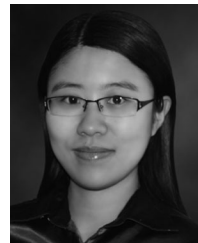
Nan Yan is currently working as a third year undergraduate student in the Department of Automation, Tsinghua University. His research interests are mainly on the intelligent unmanned system and perception for robotics.



Deng Luo (S'16) received the B.S. degree in electronic engineering from the Huazhong University of Science and Technology, Wuhan, China, in 2014. He is currently working toward the Ph.D. degree with Tsinghua University, Beijing, China, focusing on low-noise, low-power, and low-voltage analog circuit design. His research interests include analog and mixed-signal circuit designs, especially for biomedical applications.



Yiqiao Liao (S'17) received the B.S. degree in microelectronics from the Hefei University of Technology, HeFei, China, in 2014. He is currently working toward the Ph.D. degree with Tsinghua University, Beijing, China, focusing on biomedical signal processing and deep learning. His research interests include domain adaption and transfer learning, especially for biomedical signal processing.



Milin Zhang (S'06–M'11–SM'17) received the B.S. and M.S. degrees in electronic engineering from Tsinghua University, Beijing, China, in 2004 and 2006, respectively, and the Ph.D. degree from the Electronic and Computer Engineering Department, The Hong Kong University of Science and Technology (HKUST), Hong Kong. She was a Postdoctoral Researcher with the University of Pennsylvania, Philadelphia, PA, USA. In 2016, she joined the Department of Electronic Engineering, Tsinghua University, as an Assistant Professor. Her research interests include designing traditional and various nontraditional imaging sensors, such as polarization imaging sensors and focal-plane compressive acquisition image sensors. She is also interested in analog and mixed-signal circuit designs oriented for various applications. Dr. Zhang has been serving as a Technology Program Committee Member of the IEEE Asian Solid-State Circuits Conference (A-SSCC) since 2019, the IEEE Custom Integrated Circuits Conference (CICC) since 2018, and the IEEE International Solid-State Circuits Conference Student Research Preview (ISSCC SRP) Committee. She received the Best Paper Award of the BioCAS Track of the 2014 International Symposium on Circuits and Systems (ISCAS) and the Best Paper Award (first place) of the 2015 Biomedical Circuits and Systems Conference (BioCAS).



Zhihua Wang (M'99–SM'04–F'17) received the B.S., M.S., and Ph.D. degrees in electronic engineering from Tsinghua University, Beijing, China, in 1983, 1985, and 1990, respectively. He was a Visiting Scholar with Carnegie Mellon University, Pittsburgh, PA, USA, from 1992 to 1993 and Katholieke Universiteit Leuven, Leuven, Belgium, from 1993 to 1994. He has been serving as a Full Professor and the Deputy Director of the Institute of Microelectronics, Tsinghua University, since 1997 and 2000, respectively. He was a Visiting Professor with The Hong Kong University of Science and Technology, Hong Kong, from 2014 to 2015. He has coauthored 12 books/chapters, over 197 (514) papers in international journals (conferences), and over 246 (29) papers in Chinese journals (conferences). He holds 118 Chinese and 9 U.S. patents. His current research mainly focuses on CMOS radio frequency integrated circuit (RFIC) and biomedical applications, involving radio frequency identification (RFID), phase-locked loop, low-power wireless transceivers, and smart clinic equipment combined with leading-edge RFIC and digital image processing techniques. Dr. Wang has been a Steering Committee Member of the IEEE Asian Solid-State Circuits Conference (A-SSCC) since 2005. He served as the Chairman for the IEEE SSCS Beijing Chapter from 1999 to 2009, an AdCom Member of the IEEE Solid-State Circuits Society (SSCS) from 2016 to 2019, a Technology Program Committee Member of the IEEE International Solid-State Circuits Conference from 2005 to 2011, the Technical Program Chair for A-SSCC 2013, a Guest Editor of the IEEE Journal of Solid-State Circuits special issues in 2006, 2009, and 2014, an Associate Editor of the IEEE Transactions on Circuits and Systems I and II and the IEEE Transactions on Biomedical Circuits and Systems, and other administrative/expert committee positions in China's national science and technology projects.



Xiang Xie is an Associated Professor with the Institute of Microelectronics, Tsinghua University. His research fields cover SoC design, image processing, biomedical electronics and pervasive HCI. His current main research projects includes a new generation of wireless Micro-Ball endoscopy system, portable and mobile 3D image data acquisition and processing, and SoC and DSP design for the pervasive HCI system. He is the author or co-author of more than 100 papers, two books, and one book chapter in the related research fields. He has filed over ten patents and applied for over ten patents in this research field. Especially, the first generation of wireless capsule endoscopy system based on his research fruits has been commercialized.



Anhe Wang received the Ph. D from the Institute of Chemistry, Chinese Academy of Sciences in 2010, and then moved to Radboud University Nijmegen (The Netherland) as a post-doctor. In 2016, he joined the gel-based biomaterials' group of Institute of Process Engineering, Chinese Academy of Sciences as an Associate Professor. His interests include the designing and fabricating multifunctional nano/micro-gels as excellent carriers in drug delivery. He is also interested in self-assembly behavior of short peptide and 3D bio-printing.



Yang Chen received the B.S. degree in School of Biotechnology, Jiangnan University, Jiangsu, China, in 2018. He is currently working toward the M.S. degree with the Institute of Process Engineering, Chinese Academy of Sciences, focusing on the designing and fabrication of biomaterial film based on silk protein and short peptides. His research interests include soft substrate preparation and flexible device designing, especially for biomedical applications.



Shuo Bai received the B.S. degree from Peking University, Beijing, China in 2004, and the M.S. degree from Humboldt-Universität zu Berlin, Germany, in 2007. Then he received the Ph.D degree from Max Planck Institute of Colloids and Interfaces in 2010. Thereafter, he moved to Adophe Merkle Institute and University of Strathclyde as a post-doctor and assisted professor in 2011 and 2012, respectively. Now, he is a full professor in Institute of Process Engineering, Chinese Academy of Sciences, focusing on the designing and application of biomaterials. His research interests include designing of supramolecular and polymeric hydrogels, gel-based systems for biomimetics, biocatalyzing and drug delivery carriers, functional gels, and 3D bio-printing technology.